Silicon Photomultipliers Signal-to-Noise Ratio in the Continuous Wave Regime

Gabriele Adamo, Antonino Parisi, Salvatore Stivala, Alessandro Tomasino, Diego Agrò, Luciano Curcio, Giuseppe Costantino Giaconia, Alessandro Busacca, and Giorgio Fallica

***Abstract*—We report on signal-to-noise ratio measurements carried out in the continuous wave regime, at different bias voltages, frequencies, and temperatures, on a class of silicon photomultipliers fabricated in planar technology on silicon p-type substrate. Signal-to-noise ratio has been measured as the ratio of the photogenerated current, filtered and averaged by a lock-in amplifier, and the root mean square deviation of the same current. The measured noise takes into account the shot noise, resulting from the photocurrent and the dark current. We have also performed a comparison between our SiPMs and a photomultiplier tube in terms of signal-to-noise ratio, as a function of the temperature of the SiPM package and at different bias voltages. Our results show the outstanding performance of this class of SiPMs even without the need of any cooling system.**

***Index Terms*—Photodetectors, noise, photomultipliers, signal-to-noise ratio.**

I. Introduction

MEASUREMENTS of low photon fluxes require high responsivity and a remarkable signal-to-noise ratio (SNR). Besides, photodetector research is pushing towards the pixel miniaturization in order to obtain improved spatial resolution and ever smaller dimensions.

In this perspective, conventional vacuum photomultiplier tubes (PMTs) and ordinary avalanche photodiodes (APDs) will be replaced, in the near future, by silicon photomultipliers (SiPMs) [1], [2]. These photodiodes present independent photon counting microcells connected to a common analog output able to produce a summation signal proportional to the number of detected photons [3]–[9].

SiPMs have several advantages compared to PMTs: higher quantum efficiency (particularly in the near infrared), low operating voltage (<30 V), good gain ($>10^6$), very small size, reduced power requirements, reduced sensibility to voltage fluctuations and temperature, and almost complete insensitivity to magnetic fields [6]–[14]. Moreover, inexpensive SiPMs have typical advantages of the planar integration process [15], [16]. Therefore, they offer an effective and alternative solution combining the advantages of PMTs and APDs. In fact, solid-state technology and improved integration process allowed to employ these devices in medical imaging systems, such as positron emission tomography [17]–[20]. High gain, excellent timing properties, and insensitivity to magnetic fields could guarantee new SiPM applications in several fields.

At the present time, SiPMs are mainly employed in photon counting mode, in conjunction with pulsed lasers [1]–[3], [10]–[16], [21], [22] and, therefore, the dark noise is the main noise source. However, SiPMs can be used in the continuous wave (CW) regime in several applications, such as very low power measurements (less than 1 pW) [23], as disposable sensors in immunoassay tests [24] and, above all, in CW near-infrared spectroscopy systems [25]–[32]. For this reason, it is important to investigate the effect of SNR in these operative conditions [33]–[35]. In the CW regime, at very low optical intensities, the shot noise component, arising from photon statistical fluctuations, must be taken into account [27], [36], [37].

In this paper, SNR measurements on a class of SiPMs have been carried out. This characterization has been performed in the CW regime as a function of the applied bias, of the reference frequency and of the temperature of the SiPM package. Furthermore, the same measurements have been performed on a PMT, thus obtaining a comparison between these two classes of devices in terms of SNR.

II. Description of the Device

SiPM fabrication technology is based on single-photon avalanche diode (SPAD) pixels. The SiPM device has been designed with a 3.5 × 3.5 mm^2 active area, encased in a 5 × 5.5 mm^2 package, and consist of a 3600 SPAD array (60 × 60 pixels) with a 58 μm pixel pitch size, a 45% fill factor and a breakdown voltage (BV) of about 28.0 V.

Each SPAD needs a quenching circuit obtained via a low doped polysilicon resistor. The latter is present in each single pixel [38] and has a value of 256 kΩ. The series of each SPAD and its quenching resistor are connected in parallel. Details about the fabrication are extensively explained in [33].

III. Experimental Results and Data Analysis

A. Electrical Characterization

An electrical characterization of the SiPM has been carried out in forward and reverse current, by using a Keithley

Manuscript received January 31, 2014; revised July 11, 2014; accepted August 1, 2014. Date of publication August 8, 2014; date of current version September 1, 2014. This work was supported in part by the Project High Profile (HIGH-throughput PROduction of FunctIonaL 3-D imagEs of the brain under Grant 269356), which is funded by the European Community under the Artemis Joint Undertaking scheme.

G. Adamo, A. Parisi, S. Stivala, A. Tomasino, D. Agrò, L. Curcio, G. C. Giaconia, and A. Busacca are with the Department of Energy, Information Engineering and Mathematical Models, University of Palermo, Palermo 90128, Italy (e-mail: gabriele.adamo@unipa.it; antonino.parisi@unipa.it; salvatore.stivala@unipa.it; alessandro.tomasino87@gmail.com; diego.agro@unipa.it; luciano.curcio@unipa.it; costantino.giaconia@unipa.it; alessandro.busacca@unipa.it).

G. Fallica is with the Department of Research and Development IMS, STMicroelectronics, Catania 95121, Italy (e-mail: giorgio.fallica@st.com).

Color versions of one or more of the figures in this paper are available online at http://ieeexplore.ieee.org.

Digital Object Identifier 10.1109/JSTQE.2014.2346489

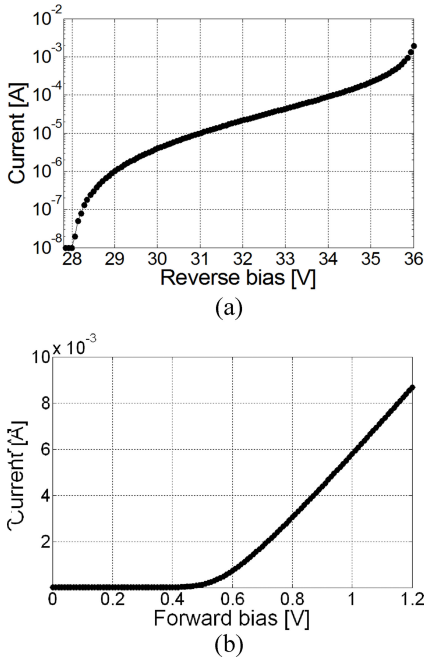

Fig. 1. (a) Reverse and (b) forward *I–V* SiPM characteristics measured at room temperature and in dark conditions.

2440 semiconductor parameter analyzer. These measurements were performed at controlled room temperature and in dark conditions.

Below the BV, a reverse current significantly less than 10 nA is observed [see Fig. 1(a)] [33]. This is in agreement with the level of dark current measured in these devices at room temperature. At a reverse bias value of 28.0 V, the BV is reached and a steep increase of the SiPM generated current is observed. In particular, the steepest slope is approximately located within the first volt above the breakdown, while a linear behavior of the *I–V* characteristic (on semilogarithmic scale) is detected from 30 to 35 V [see Fig. 1(a)] [33]. In forward bias [see Fig. 1(b)], above the threshold of 0.6 V, the current is limited by the quenching resistor [39]. Therefore, its value can be extrapolated by measuring the slope of the linear region, resulting in a value of 71 Ω for the overall SiPM quenching resistor. Indeed, such an equivalent resistor corresponds to the parallel of all the 256 kΩ quenching resistors [33].

B. SNR Measurements

Noise in SiPMs is mainly due to shot noise and thermal noise [13].

As regards the shot noise, because of statistical fluctuations of both the photogeneration and the thermal-generation processes, the average overall current flowing through the SiPM (I_o) includes a superimposed ac component. The total generation rate is a random variable with a Poissonian probability distribution, so that the spectral density of its noise is $2eI_o$, where e is the electron charge [40], [41]. Therefore, the overall shot noise current i_o (RMS) is given by

$$i_o = \sqrt{2eI_oFB\mu} \tag{1}$$

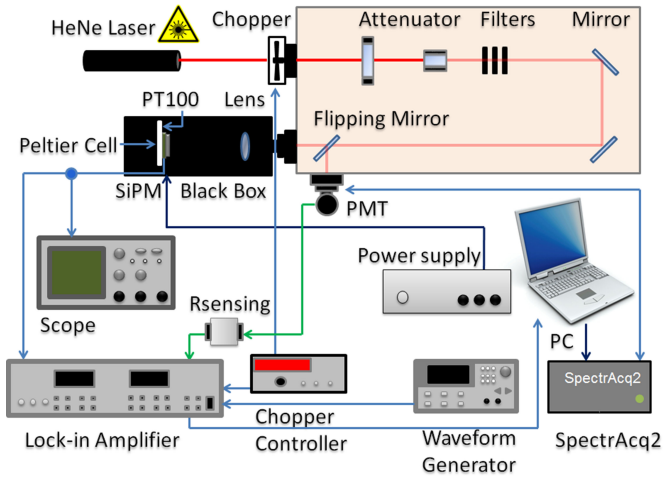

Fig. 2. Sketch of the experimental setup for measurements of the SiPM SNR.

where F is the excess noise Factor of the SiPM, B is the frequency bandwidth of the noise measurement system and μ is the gain of the SiPM.

In more detail, the overall shot noise is given by the shot noise of each component of the current, i.e., signal (i_s), dark (i_d) and background (i_b) shot noise currents, given by (RMS values)

$$i_n = \sqrt{2eI_nFB\mu} \quad (n = s, d, b) \tag{2}$$

where I_s, I_d and I_b are the average signal, dark and background currents, respectively.

The presence of F in (1) and (2) and its physical meaning can be explained as follows. In SiPMs, pixel-to-pixel gain variations, cross-talk (due to the migration of photons towards neighboring pixels) and afterpulsing [13] (caused by trapping centers in the depletion region), introduce an increased noise contribute. This multiplication noise can be numerically expressed—in a similar way as usually done for PMTs and APDs operated below breakdown—in terms of the "excess noise factor", F [42].

As stated above, another cause of noise in SiPMs is the thermal noise. In addition to the real signal, electron/hole pairs can also be generated in the SiPM depletion region because of either thermal generation of carriers through shockley-read-hall recombination-generation centers or bulk diffusion of minority carriers from the quasi-neutral region. Generation of electron/hole pairs and bulk diffusion represents the characteristic thermal noise of this type of devices and, being undistinguishable from the real signal, sets a limit for the ultimate sensitivity in SiPMs. In the absence of light, the electrical effect of these mechanisms is referred to as dark current (showing an average value named I_d) [5].

The experimental setup, employed for our continuous wave SNR measurements, is shown in Fig. 2. The optical power provided by a HeNe laser ($\lambda = 632.8$ nm) was attenuated by means of some neutral density filters and controlled through a half-wave plate and a Glan–Thompson cube polarizer. This system allowed us to finely tune the optical power down to few picowatts. The laser beam was sent either on the SiPM active area under test or on a reference PMT (Hamamatsu R928)—

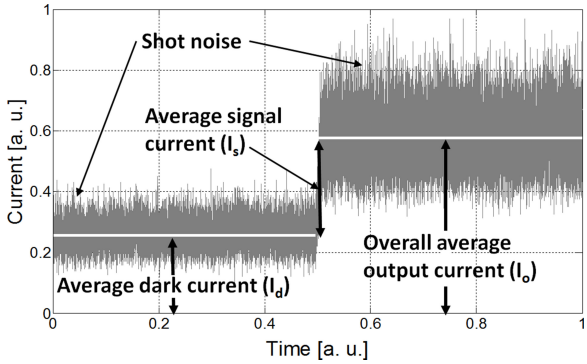

Fig. 3. Temporal trend of the SiPM response to the chopped optical beam, as observed at the oscilloscope. Signal and noise contributions have been indicated.

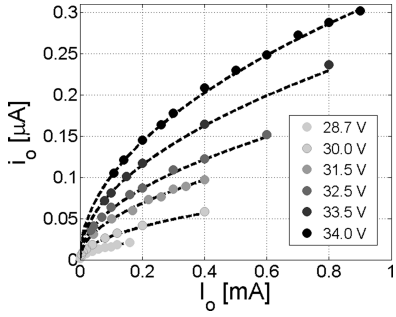

Fig. 4. Overall shot noise current i_o, as a function of the average overall current I_o, at different biases.

previously calibrated and used to estimate the optical power incident on the SiPM—depending on the position of a flipping mirror.

The SiPM was biased using a stabilized power supply and a SMD resistor (50 Ω, sensing resistor), connected between the cathode and the ground. This resistance is in parallel with the input resistance of the measurement system (100 MΩ), thus providing an equivalent resistance of $R_{eq} \approx 50\ \Omega$.

The SiPM and the biasing circuit were located in a metal black box, being thus shielded from ambient light and electromagnetic noise. A 25-mm focal length lens was placed between the flipping mirror and the SiPM, making sure that the light spot covered the whole active area of the device. During measurements, the temperature of the SiPM package was controlled through a Peltier cell placed in the back side of the device, whereas a PT100 thermistor allowed us to record the temperature of the SiPM package. In order to perform low optical power measurements, a lock-in amplifier was connected to both the SiPM and the PMT outputs, while a readout system (SpectrAcq2) digitized the signal and allowed data acquisition [34].

Following our set-up description, we can underline that some of the above-mentioned noise contributions are negligible. In particular, since background light is not present in our setup, i_b is close to zero.

Furthermore, the noise coming from the resistance R_{eq} provides a contribution given by

$$i_e = \sqrt{\frac{4k_B T B}{R_{\mathrm{eq}}}} \tag{3}$$

where k_B is the Boltzman constant, and *T* is the absolute temperature. This contribution is negligible with respect to the measured shot noise currents for all our experimental conditions. It is also worth noting that the electronic noise introduced by the measurement system can be neglected.

On the other hand, noise contributions provided by the shot noise of the signal current (i_s) and the shot noise of the dark current (i_d), as well as the thermal noise (i.e., average dark current I_d), need to be taken into account. A typical temporal trend of the SiPM response to a chopped optical beam, as observed at the oscilloscope, is shown in Fig. 3, where signal and noise contributions have been highlighted.

Unlike the shot noise, SiPM average dark current is an offset term and it can be filtered through a simple external dc removal circuit. For this reason, in our paper, we focus the attention on the SNR measurements, expressed by the ratio of the SiPM average signal (photogenerated) current I_s and the RMS deviation of the overall current (i.e., the overall shot noise current i_o).

We employed a lock-in amplifier and an optical chopper system (working at a frequency of 183 Hz) in order to acquire I_s after noise removal, while I_o and I_d were acquired via a multimeter. The RMS deviation was provided by the lock-in amplifier set in the "noise measurement" mode. We employed a $B = 10$ Hz equivalent noise bandwidth, around the lock-in amplifier reference frequency, the latter supplied by a waveform generator. The measured noise only takes into account the shot noise, resulting from the photocurrent and the dark current.

SNR measurements were performed with a constant incident optical power of 11 pW, so to be sure that the SiPM behavior was linear up to, at least, 35.3 V [33].

Fig. 4 illustrates our measurements of i_o as a function of I_o at different overvoltages (OVs, i.e., volts above breakdown). The interpolation of such data follows a square root trend, in good agreement with (1).

From data shown in Fig. 4, the product $F{\cdot}\mu$ has been extrapolated for each OV value. In order to determine *F*, we have performed SiPM gain measurements. We employed a PiLas laser with 405 nm emission wavelength and 40 ps pulse duration (full width at half maximum). Variable neutral density filters and an optical disk diffuser allowed us to both reduce the light intensity and to uniformly illuminate the active area of the SiPM. The laser beam was constantly monitored during the characterization by means of a calibrated reference diode. The output charge spectra were acquired through a CAEN QDC V965A connected to a PC via a CAEN V 1718 USB bridge, both inserted in a CAEN VME 8002 crate (without using any amplification stage). Signals were visualized through a 1 GHz bandwidth oscilloscope.

The gain value was extrapolated from single photoelectron charge spectra [4] obtained with an integration time of 400 ns. The integration window was set to completely integrate the pulse shape of the SiPM under test.

For each photoelectron peak, a histogram, representing the distribution of the associated avalanche charge, was produced. Each histogram was fitted with a Gaussian function (of variance

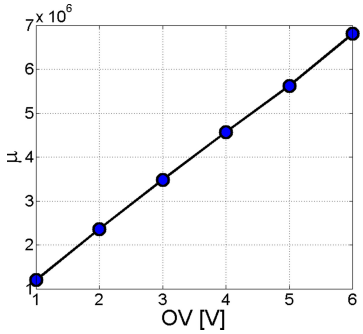

Fig. 5. Gain measurements at different OVs and their linear best fit.

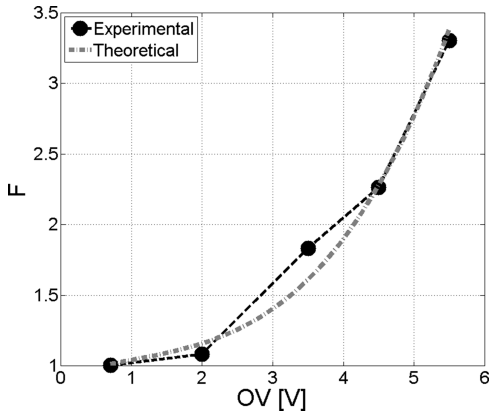

Fig. 6. Excess Noise factor at different OVs.

σ_μ^2), whose centroid represents the average charge associated to the corresponding peak. The charge increment between adjacent photoelectron peaks exactly corresponds to the output charge of one detected photon. The gain μ was obtained dividing this quantity by the electron elementary charge [4]. Fig. 5 shows μ as a function of the applied OV and its linear best fit. Following the measurements shown in Fig. 4 and gain measurements, we calculated the values of F at different OVs. As shown in Fig. 6, *F* increases with the OV. This trend cannot be due to the portion of the excess noise factor coming from pixel-to-pixel gain fluctuations ($F_{\rm p}$) calculated from the single electron distribution, by using

$$F_p = \sqrt{1 + \frac{\sigma_\mu^2}{\mu^2}} \tag{4}$$

where σ_μ^2 is the variance of the SiPM gain μ [42]. Indeed, employing (4), we obtained a quasi-constant value of $F_p (F_p \approx 1.004)$ in all the examined OV range (up to $\mathrm{OV} = 5.5$ V). This means that the abovementioned gain fluctuations can be considered reasonably small for the photodetector under test.

On the other hand, the increase of *F* [42] can be ascribed more to optical crosstalk than to afterpulsing. Even if the crosstalk probability can be only slightly higher than the afterpulsing probability, it is important to focus on their charge contributions. Indeed, the charge contribution of the former is about four times the charge contribution of the latter [43].

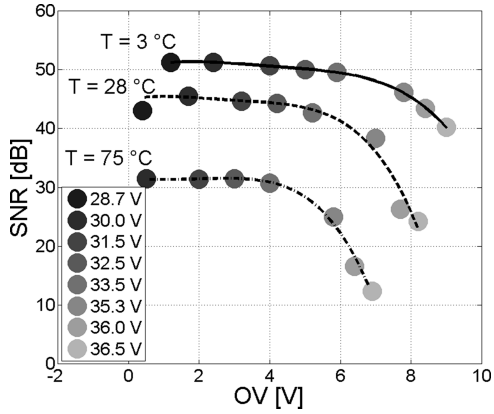

Fig. 7. SiPM SNR versus applied OV at $\lambda = 632.8$ nm, at three different temperatures (3, 28, 75 °C) of the SiPM package and employing an equivalent noise bandwidth of 10 Hz. The legend shows the applied reverse bias voltages. The lines are best-fit curves for the experimental data at the temperature of 3, 28 and 75 °C, respectively. These results do not change in the frequency range (1–100 kHz).

Data reported in Fig. 6 are in good agreement with the theoretical expression (5) of *F* [44]

$$F \cong 1 + P + \frac{3}{2}P^2 + o(P^3) \tag{5}$$

where *P* is a quadratic crosstalk probability as a function of the OV, given by (6) [45]

$$P = k\mathrm{OV}^2. \tag{6}$$

As shown in Fig. 6, we obtained the best-fit of our *F* measurements with $k = 3.2 \times 10^{-2}$ up to $\mathrm{OV} = 5.5$ V. Such a choice for k provides *P* values that are comparable to what previously reported in literature. For example, at $\mathrm{OV} = 3$ V, P is 16.1% (i.e., 12.8% + 3.3%, sum of crosstalk and afterpulsing probabilities, respectively) in [43], while it results 28% in our analysis.

Fig. 7 shows the SiPM SNR versus the applied OV at $\lambda = 632.8$ nm and at three different temperatures (3, 28, 75 °C) of the SiPM package. The legend shows the applied reverse bias voltages between the anode and the cathode of the device, while the applied OV, depicted in the *x*-axis, has been estimated taking into account the BV shift with temperature ($\mathrm{BV} = 28.0$ V at room temperature). The same figure exhibits a quasi-flat trend up to an OV of about 5 V. This is what we expected, indeed, at low OVs, the increase of F can be neglected (see Fig. 6) if compared to the increase of μ and I_o. I_s, I_o and μ are proportional to the OV. As a consequence (see Eq. 1), also i_o is proportional to the OV. Hence, both the numerator (I_s) and the denominator (i_o) of SNR grow linearly with the OV and, therefore, we expect SNR exhibits a flat trend as confirmed by our measurements.

At higher OVs, we have observed the SNR decrease, because of the strong increase of the shot noise and of F and the decrease of the signal current.

Fig. 8 depicts the SNR of the investigated SiPM as a function of its package temperature and at different bias voltages. In the case of room temperature, we have also compared the SiPM SNR with the SNR of a PMT (Hamamatsu R928). SiPM

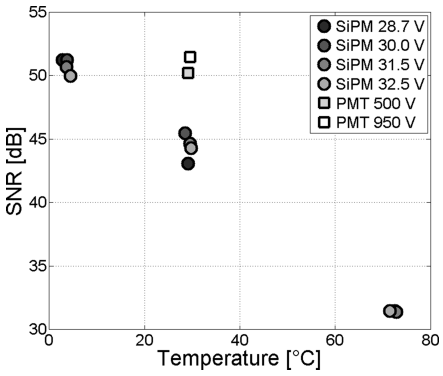

Fig. 8. SiPM SNR versus temperature of the SiPM package, employing an equivalent noise bandwidth of 10 Hz. SNR measurements performed on the reference PMT at room temperature are plotted to make a comparison. The legend shows the applied bias voltages. These results do not change in the considered frequency range (1–100 kHz).

performances are outstanding, since its SNR is only ≈ 6–7 dB below the PMT SNR, at the same temperature. Moreover, cooling the SiPM package, by means of a Peltier cell, at a temperature of 3 °C, it reaches the PMT SNR values. Such a result has been achieved biasing the SiPM up to 32.5 V against a bias up to 950 V for the PMT. Finally, we repeated our measurements at different lock-in amplifier reference frequencies in the range 1–100 kHz. We have found the same results shown above and, therefore, we can conclude that SiPM SNR is constant in the explored frequency range.

IV. Conclusion

In this paper, we reported on the electrical and the optical characterization in terms of SNR, in the CW regime, of a class of SiPM, fabricated on a silicon p-type substrate. In particular, we have shown, for the first time, our SiPM SNR measurements as a function of the applied bias, of the reference frequency and of the temperature of the SiPM package. Similar measurements were also performed on a PMT, in order to make a comparison. A 10 Hz equivalent noise bandwidth was employed, around the lock-in amplifier reference frequency. Furthermore, excess noise factor measurements were performed and explained.

Our results highlight the outstanding performance of this class of SiPMs, even without the need of any cooling system. Indeed, their SNR is only ≈ 6–7 dB below the PMT SNR at room temperature. Furthermore, cooling the SiPM package at a temperature of the Peltier cell of 3 °C, it reaches the PMT SNR values at room temperature, even if the SiPM is biased in the range of 28.7–33.5 V, against a bias value up to 950 V of the PMT.

References

[1] G. Collazuol, G. Ambrosi, M. Boscardin, F. Corsi, G. F. Dalla Betta, A. Del Guerra, N. Dinu, M. Galimberti, D. Giulietti, L. A. Gizzi, L. Labate, G. Llosa, S. Marcatili, F. Morsani, C. Piemonte, A. Pozza, L. Zaccarelli, and N. Zorzi, "Single photon timing resolution and detection efficiency of the IRST silicon photo-multipliers," *Nucl. Instrum. Methods Phys. Res. A*, vol. 581, nos. 1/2, pp. 461–464, Aug. 2007.

[2] F. Zappa, S. Tisa, A. Tosi, and S. Cova, "Principles and features of single-photon avalanche diode arrays," *Sens. Actuators A, Phys.*, vol. 140, no. 1, pp. 103–112, Oct. 2007.

[3] P. Buzhan, B. Dolgoshein, L. Filatov, A. Ilyin, V. Kantzerov, V. Kaplin, A. Karakash, F. Kayumov, S. Klemin, E. Popova, and S. Smirnov, "Silicon photomultiplier and its possible applications," *Nucl. Instrum. Methods Phys. Res. A*, vol. 504, nos. 1–3, pp. 48–52, Mar. 2003.

[4] M. Mazzillo, G. Condorelli, D. Sanfilippo, G. Valvo, B. Carbone, G. Fallica, S. Billotta, M. Belluso, G. Bonanno, L. Cosentino, A. Pappalardo, and P. Finocchiaro, "Silicon photomultiplier technology at STMicroelectronics," *IEEE Trans. Nucl. Sci.*, vol. 56, no. 4, pp. 2434–2442, Aug. 2009.

[5] V. Golovin and V. Saveliev, "Novel type of Avalanche photodetector with Geiger mode operation," *Nucl. Instrum. Methods Phys. Res. A*, vol. 518, nos. 1/2, pp. 560–564, Feb. 2004.

[6] M. Mazzillo, A. Piazza, G. Condorelli, D. Sanfilippo, G. Fallica, S. Billotta, M. Belluso, G. Bonanno, L. Cosentino, A. Pappalardo, and P. Finocchiaro, "Quantum detection efficiency in Geiger mode avalanche photodiodes," *IEEE Trans. Nucl. Sci.*, vol. 55, no. 6, pp. 3620–3625, Dec. 2008.

[7] M. Mazzillo, G. Condorelli, D. Sanfilippo, A. Piazza, G. Valvo, B. Carbone, G. Fallica, A. Pappalardo, L. Cosentino, P. Finocchiaro, M. Corselli, G. Suriani, S. Lombardo, S. Billotta, M. Belluso, and G. Bonanno, "Silicon photomultipliers for nuclear medical imaging applications," *Proc. SPIE*, vol. 7003, pp. 70030I–1–70030I-11, Apr. 2008.

[8] G. Giustolisi, G. Palumbo, P. Finocchiaro, and A. Pappalardo, "A simple extraction procedure for determining the electrical parameters in silicon photomultipliers," in *Proc. Eur. Conf. Circuit Theory Des.*, Sep. 2013, pp. 1–4.

[9] G. Giustolisi, R. Mita, and G. Palumbo, "Behavioral modeling of statistical phenomena of single-photon avalanche diodes," *Int. J. Circuit Theoy. Appl.*, vol. 40, no. 7, pp. 661–679, Jul. 2012.

[10] B. Dolgoshein, V. Balagura, P. Buzhan, M. Danilov, L. Filatov, E. Garutti, M. Groll, A. Ilyin, V. Kantserov, V. Kaplin, A. Karakash, F. Kayumov, S. Klemin, V. Korbel, H. Meyer, R. Mizuk, V. Morgunov, E. Novikov, P. Pakhlov, E. Popova, V. Rusinov, F. Sefkow, E. Tarkovsky, and I. Tikhomirov, "Status report on silicon photomultiplier development and its applications," *Nucl. Instrum. Methods Phys. Res. Sect. A, Accel., Spectrometers, Detectors Assoc. Equip.*, vol. 563, no. 2, pp. 368–376, Jul. 2006.

[11] V. D. Kovaltchouk, G. J. Lolos, Z. Papandreou, and K. Wolbaum, "Comparison of a silicon photomultiplier to a traditional vacuum photomultiplier," *Nucl. Instrum. Methods Phys. Res. Sect. A, Accel., Spectrometers, Detectors Assoc. Equip.*, vol. 538, nos. 1–3, pp. 408–415, Feb. 2005.

[12] A. Pasquazi, A. Busacca, S. Stivala, R. Morandotti, and G. Assanto, "Nonlinear disorder mapping through three-wave mixing," *IEEE Photon. J.*, vol. 2, no. 1, pp. 18–28, Feb. 2010.

[13] P. Finocchiaro, A. Pappalardo, L. Cosentino, M. Belluso, S. Billotta, G. Bonanno, B. Carbone, G. Condorelli, S. Di Mauro, G. Fallica, M. Mazzillo, A. Piazza, D. Sanfilippo, and G. Valvo, "Characterization of a novel 100-channel silicon photomultiplier—Part I: Noise," *IEEE Trans. Electron Devices*, vol. 55, no. 10, pp. 2757–2764, Oct. 2008.

[14] A. Parisi, A. C. Cino, A. C. Busacca, M. Cherchi, S. Riva-Sanseverino, "Integrated optic surface plasmon resonance measurements in a borosilicate glass substrate," *Sensors*, vol. 8, no. 11, pp. 7113–7124, Nov. 2008.

[15] G. Barbarino, R. de Asmundis, G. De Rosa, C. M. Mollo, S. Russo, and D. Vivolo, *Silicon Photo Multipliers Detectors Operating in Geiger Regime: An Unlimited Device for Future Applications*. Vukovar, Croatia: InTech, Jul. 2011.

[16] M. Mazzillo, G. Condorelli, D. Sanfilippo, G. Valvo, B. Carbone, A. Piana, G. Fallica, A. Ronzhin, M. Demarteau, S. Los, and E. Ramberg, "Timing performances of large area silicon photomultipliers fabricated at STMicroelectronics," *IEEE Trans. Nucl. Sci.*, vol. 57, no. 4, pp. 2273–2279, Aug. 2010.

[17] N. Efthimiou, G. Argyropoulos, G. Panayiotakis, M. Georgiou, and G. Loudos, "Initial results on SiPM performance for use in medical imaging," in *Proc. IEEE Int. Conf. Imag. Syst. Tech.*, Jul. 2010, pp. 256–260.

[18] D. J. Herbert, V. Saveliev, N. Belcari, N. D'Ascenzo, A. Del Guerra, and A. Golovin, "First results of scintillator readout with silicon photomultiplier," *IEEE Trans. Nucl. Sci.*, vol. 53, no. 1, pp. 389–394, Feb. 2006.

[19] P. Buzhan, B. Dolgoshein, L. Filatov, A. Ilyin, V. Kaplin, A. Karakash, S. Klemin, R. Mirzoyan, A. N. Ottec, E. Popova, V. Sosnovtsev, and M. Teshima, "Large area silicon photomultipliers: Performance and applications," *Nucl. Instrum. Methods Phys. Res. Sect. A, Accel., Spectrometers, Detectors Assoc. Equip.*, vol. 567, no. 1, pp. 78–82, Jun. 2006.

[20] E. Roncali and S. R. Cherry, "Application of silicon photomultipliers to positron emission tomography," *Ann. Biomed. Eng.*, vol. 39, no. 4, pp. 1358–1377, Feb. 2011.
[21] M. Cherchi, A. Taormina, A. C. Busacca, R. L. Oliveri, S. Bivona, A. C. Cino, S. Stivala, S. R. Sanseverino, and C. Leone, "Exploiting the optical quadratic nonlinearity of zinc-blende semiconductors for guidedwave terahertz generation: A material comparison," *IEEE J. Quantum Electron.*, vol. 46, no. 3, pp. 368–376, Mar. 2010.
[22] A. Tomasino, A. Parisi, S. Stivala, P. Livreri, A. C. Cino, A. C. Busacca, M. Peccianti, and R. Morandotti, "Wideband THz time domain spectroscopy based on optical rectification and electro-optic sampling," *Sci. Rep.*, vol. 3, pp. 3116–3123, Oct. 2013.
[23] P. Eraerds, M. Legré, A. Rochas, H. Zbinden, and N. Gisin, "SiPM for fast photon-counting and multiphoton detection," *Opt. Exp.*, vol. 15, no. 22, pp. 14539–14549, Oct. 2007.
[24] E. Matveeva, J. Malicka, I. Gryczynski, Z. Gryczynski, and J. R. Lakowicz, "Multi-wavelength immunoassays using surface plasmon-coupled emission," *Biochem. Biophys. Res. Commun.*, vol. 313, no. 3, pp. 721–726, Jan. 2004.
[25] D. Contini, A. Torricelli, A. Pifferi, L. Spinelli, P. Taroni, V. Quaresima, M. Ferrari, and R. Cubeddu, "Multichannel time-resolved tissue oximeter for functional imaging of the brain," *IEEE Trans. Instrum. Meas.*, vol. 55, no. 1, pp. 85–90, Feb. 2006.
[26] M. Nitzan and H. Taitelbaum, "The measurement of oxygen saturation in arterial and venous blood," *IEEE Instrum. Meas. Mag.*, vol. 11, no. 3, pp. 9–15, Jun. 2008.
[27] D. Haensse, "A new multichannel near infrared spectrophotometry system for functional studies of the brain in adults and neonates," *Opt. Exp.*, vol. 13, no. 12, pp. 4525–4538, Jun. 2005.
[28] T. Achtnich and F. Braun, "Design and evaluation of a modular fNIRS probe for employment in neuroimaging applications," Master's thesis, Eidgenössische Technische Hochschule Zürich, Institut für Biomedizinische Technik, Zürich, Switzerland, 2012.
[29] F. Zou, C. Jin, R. R. Ross, and B. Soller, "Investigation of spectral interferences on the accuracy of broadband CW-NIRS tissue SO_2 determination," *Biomed. Opt. Exp.*, vol. 1, no. 3, pp. 748–761, Oct. 2010.
[30] K. J. Kek, R. Kibe, M. Niwayama, N. Kudo, and K. Yamamoto, "Optical imaging instrument for muscle oxygenation based on spatially resolved spectroscopy," *Opt. Exp.*, vol. 16, no. 22, pp. 18173–18187, Oct. 2008.
[31] G. Salvatori, K. I. Suh, R. R. Ansari, and L. Rovati, "Instrumentation and calibration protocol for a continuous wave near infrared hemoximeter," *IEEE Trans. Instrum. Meas.*, vol. 55, no. 4, pp. 1368–1376, Aug. 2006.
[32] R. Pernice, G. Adamo, S. Stivala, A. Parisi, A. Busacca, D. Spigolon, M. A. Sabatino, L. D'Acquisto, and C. Dispenza, "Opals infiltrated with a stimuli-responsive hydrogel for ethanol vapor sensing," *Opt. Mater. Exp.*, vol. 3, no. 11, pp. 1820–1833, Nov. 2013.
[33] G. Adamo, D. Agrò, S. Stivala, A. Parisi, G. C. Giaconia, A. Busacca, M. Mazzillo, D. Sanfilippo, and G. Fallica, "Measurements of Silicon photomultipliers responsivity in continuous wave regime," *IEEE Trans. Electron. Dev.*, vol. 60, no. 11, pp. 3718–3725, Nov. 2013.
[34] G. Adamo, D. Agrò, S. Stivala, A. Parisi, C. Giaconia, A. C. Busacca, M. Mazzillo, D. Sanfilippo, and G. Fallica, "Responsivity measurements of N-on-P and P-on-N silicon photomultipliers in the continuous wave regime" *Proc. SPIE*, vol. 8629, pp. 86291A–1–86291A-9, Mar. 2013.
[35] G. Adamo, D. Agro', S. Stivala, A. Parisi, L. Curcio, A. Ando', A. Tomasino, C. Giaconia, A. C. Busacca, M. C. Mazzillo, D. Sanfilippo, P. G. Fallica, "Responsivity measurements of 4H-SiC Schottky photodiodes for UV light monitoring," *Proc. SPIE*, vol. 8990, pp. 899017-1–899017-7, Mar. 2014.
[36] Hamamatsu Photonics K.K. (1998, May). Photon counting using photomultiplier tubes. [Online]. Available: http://mccombe.physics.buffalo.edu/lab-manuals/photoncounting.pdf
[37] Sensl. (2008, Aug. 18). Noise in silicon photomultipliers and vacuum photomultiplier tubes. [Online]. Available: http://www.photonicsonline.com/doc/noise-in-silicon-photomultipliers-and-vacuum-0003
[38] G. Condorelli, D. Sanfilippo, G. Valvo, M. Mazzillo, D. Bongiovanni, A. Piana, B. Carbone, and G. Fallica, "Extensive electrical model of large area silicon photomultipliers," *Nucl. Instrum. Methods Phys. Res. Sec. A, Accel., Spectrometers, Detectors Assoc. Equip.*, vol. 654, no. 1, pp. 127–134, Feb. 2011.
[39] F. Corsi, C. Marzocca, A. Perrotta, A. Dragone, M. Foresta, A. Del Guerra, S. Marcatili, G. Llosa, G. Collazzuol, G.-F. Dalla Betta, N. Dinu, C. Piemonte, G. U. Pignatel, and G. Levi, "Electrical characterization of silicon photo-multiplier detectors for optimal front-end design," in *Proc. IEEE Nucl. Sci. Symp. Conf. Rec.*, Nov. 2006, pp. 276–1280.
[40] R. J. McIntyre, "A new look at impact ionization—Part I: A theory of gain, noise, breakdown probability, and frequency response," *IEEE Trans. Electron Device*, vol. 46, no. 8, pp. 1623–1631, Aug. 1999.
[41] P. Yuan, K. A. Anselm, C. Hu, H. Nie, C. Lenox, A. L. Holmes, B. G. Streetman, J. C. Campbell, and R. J. McIntyre, "A new look at impact ionization—Part II: Gain and noise in short avalanche photodiodes," *IEEE Trans. Electron Device*, vol. 46, no. 8, pp. 1632–1639, Aug. 1999.
[42] Y. Musienko, S. Reucroft, and J. Swain, "The gain, photon detection efficiency and excess noise factor of multi-pixel Geiger-mode avalanche photodiodes," *Nucl. Instrum. Methods Phys. Res. A*, vol. 567, pp. 57–61, Jun. 2006.
[43] F. Nagy, M. Mazzillo, L. Renna, G. Valvo, D. Sanfilippo, B. Carbone, A. Piana, G. Fallica, and J. Molnár, "Afterpulse and delayed crosstalk analysis on a STMicroelectronics silicon photomultiplier," *Nucl. Instrum. Methods Phys. Res. A*, vol. 759, pp. 44–49, May 2014.
[44] S. Vinogradov, "Probabilistic analysis of solid state photomultiplier performance," *Proc. SPIE*, vol. 8375, p. 83750S–1–83750S-9, May 2012.
[45] A. Vacheret, G.J. Barker, M. Dziewiecki, P. Guzowski, M.D. Haigh, B. Hartfiel, A. Izmaylov, W. Johnston, M. Khabibullin, A. Khotjantsev, Y. Kudenko, R. Kurjata, T. Kutter, T. Lindner, P. Masliah, J. Marzec, O. Mineev, Y. Musienko, S. Oser, F. Retière, R.O. Salih, A. Shaikhiev, L. F. Thompson, M. A. Ward, R. J. Wilson, N. Yershov, K. Zaremba, and M. Ziembicki, "Characterization and simulation of the response of multipixel photon counters to low light levels," *Nucl. Instrum. Methods Phys. Res. A*, vol. 656, pp. 69–83, Nov. 2011.

Gabriele Adamo received the M.Sc. degree in electronic engineering from the University of Palermo, Palermo, Italy, in 2009, where he is currently a Postdoctoral Research Fellow. His research interests include optical measurements on silicon photomultipliers.

Antonino Parisi received the M.Sc. degree in electronic engineering from the University of Palermo, Palermo, Italy, in 2000.

He is currently a Postdoctoral Research Fellow at the University of Palermo.

Salvatore Stivala received the M.Sc. degree in electronic engineering and Ph.D. degree from the University of Palermo, Palermo, Italy, in 2004 and 2008, respectively.

He is currently a Researcher at the University of Palermo.

Alessandro Tomasino received the M.Sc. degree in electronics and photonics engineering from the University of Palermo, Palermo, Italy, in 2012.

He is currently working toward the Ph.D. degree at the Faculty of Engineering, University of Palermo.

Diego Agrò received the "Laurea" degree in electronic engineering, cum laude, from the University of Palermo, Palermo, Italy, in 2011.

He is currently involved in the development of SiPM-based medical instruments in collaboration with STMicroelectronics.

Luciano Curcio received the M.Sc. degree in electronic engineering from the University of Palermo, Palermo, Italy, in 2004.

He is currently a Postdoctoral Research Fellow at the Faculty of Engineering, University of Palermo.

Giuseppe Costantino Giaconia received the Lauream degree in electronic in 1989.

He is currently an Associate Professor at the Department of Energy, Information Engineering and Mathematical Models, University of Palermo, Palermo, Italy. His research interests include optoelectronics, nanotechnologies, and digital electronics systems.

Alessandro Busacca received the "Laurea" degree in electronic engineering and Ph.D. degree from the University of Palermo, Palermo, Italy, in 1998 and 2001, respectively. He has been an Associate Professor of "electronics" at the University of Palermo.

Giorgio Fallica received the M.S. degree in physics from the University of Catania, Catania, Italy, in 1978.

He is currently the Manager of the Sensors Design Group, R&D, IMS, STMicroelectronics, Catania.